Interfacial spin-orbit torque without bulk spin-orbit coupling

Satoru Emori, Tianxiang Nan, Amine M. Belkessam, Xinjun Wang, Alexei D. Matyushov, Christopher J. Babroski, Yuan Gao, Hwaider Lin, and Nian X. Sun

Phys. Rev. B **93**, 180402 — Published 4 May 2016

DOI: 10.1103/PhysRevB.93.180402

Interfacial spin-orbit torque without bulk spin-orbit coupling

Satoru Emori,* Tianxiang Nan,† Amine M. Belkessam, Xinjun Wang, Alexei D. Matyushov, Christopher J. Babroski, Yuan Gao, Hwaider Lin, and Nian X. Sun

[1] *Department of Electrical and Computer Engineering, Northeastern University, Boston, MA 02115*

(Dated: April 12, 2016)

Abstract

An electric current in the presence of spin-orbit coupling can generate a spin accumulation that exerts torques on a nearby magnetization. We demonstrate that, even in the absence of materials with strong bulk spin-orbit coupling, a torque can arise solely due to interfacial spin-orbit coupling, namely Rashba-Eldestein effects at metal/insulator interfaces. In magnetically soft NiFe sandwiched between a weak spin-orbit metal (Ti) and insulator (Al_2O_3), this torque appears as an effective field, which is significantly larger than the Oersted field and qualitatively modified by inserting an additional layer between NiFe and Al_2O_3. Our findings point to new routes for tuning spin-orbit torques by engineering interfacial electric dipoles.

An electric current in a thin film with spin-orbit coupling can produce a spin accumulation[1–3], which can then exert sizable torques on magnetic moments[4–7]. First demonstrated in a ferromagnetic semiconductor[8], "spin-orbit torques" are nowadays studied in room-temperature ferromagnetic metals (FMs) interfaced with heavy metals (HMs) with strong spin-orbit coupling, such as Pt, Ta, and W[9–25]. These torques can arise from (1) spin-dependent scattering of conduction electrons in the bulk of the HM, i.e., the spin-Hall effect[2,3,9–13], and (2) momentum-dependent spin polarization at the HM/FM interface, i.e., the Rashba-Edelstein effect[1,5,14–17]. Since a HM/FM system can exhibit either or both of these spin-orbit effects, it can be a challenge to distinguish the spin-Hall and Rashba-Edelstein contributions[3,6,7,18,19]. Spin-orbit torques may be further influenced by spin scattering[26,27] or proximity-induced magnetization[28] at the HM/FM interface. Moreover, in many cases[9–25], the FM interfaced on one side with a HM is interfaced on the other with an insulating material, and the electric dipole at the FM/insulator interface[29,30] may also give rise to a Rashba-Edelstein effect. Recent studies[21–25] indeed suggest nontrivial influences from insulating oxide capping layers in perpendicularly-magnetized HM/FM systems. However, with the FM only $\lesssim$1 nm thick[21–25], changing the degree of oxidation of the capping layer may modify the composition of the adjacent ultrathin FM and hence the HM/FM interface. The points above make it difficult to disentangle the contributions from the HM bulk, HM/FM interface, and FM/insulator interface, thereby posing a challenge for coherent engineering of spin-orbit torques.

Here, we experimentally show a spin-orbit torque that emerges exclusively from metal/insulator interfaces in the absence of materials with strong bulk spin-orbit coupling. Our samples consist of magnetically soft $Ni_{80}Fe_{20}$ (NiFe) sandwiched between a weak spin-orbit light metal (Ti) and a weak spin-orbit insulator (Al_2O_3). We observe a "field-like" spin-orbit torque that appears as a current-induced effective field, which is significantly larger than the Oersted field. This torque is conclusively attributed to the Rashba-Edelstein effect, i.e., spin accumulation at the NiFe/Al_2O_3 interface exchange coupling to the magnetization in NiFe[4,5]. Furthermore, an insertion layer at the NiFe/Al_2O_3 interface qualitatively modifies this observed torque: Inserting an atomically thin layer of a strong spin-orbit metal (Pt) causes the field-like torque to vanish, whereas inserting a conductive weak spin-orbit metal (Cu) layer results in a "nonlocal" field-like torque where the spin accumulation couples to the magnetization in NiFe across Cu. Our findings demonstrate novel model systems exhibiting purely interfacial spin-orbit coupling, which are free from complications caused by strong spin-orbit HMs, and open possibilities for spin-orbit torques enabled by engineered electric dipoles at interfaces.

Thin-film heterostructures are sputter-deposited on Si substrates with a 50-nm thick SiO_2 overlayer. All layers are deposited at an Ar pressure of 3×10^{-3} Torr with a background pressure of $\lesssim 2\times10^{-7}$ Torr. Metallic layers are deposited by dc magnetron sputtering, whereas Al_2O_3 is deposited by rf magnetron sputtering from a compositional target. The deposition rates are calibrated by X-ray reflectivity. For each structure, unless otherwise noted, a 1.2-nm thick Ti seed layer is used to promote the growth of NiFe with narrower resonance linewidth and near-bulk saturation magnetization. Devices are patterned and contacted by Cr(3 nm)/Au(100 nm) electrodes by photolithography and liftoff.

We first examine the current-induced field in a trilayer of Ti(1.2 nm)/NiFe(2.5 nm)/Al_2O_3(1.5 nm) by using the second-order planar Hall effect (PHE) voltage technique devised by Fan *et al.*[10,11]. As illustrated in Fig. 1(a), a dc current I_{dc} along the x-axis generates a planar Hall voltage V_{PH} along the y-axis in a 100-μm wide Hall bar, which is placed in the center of a two-axis Helmholtz coil. The second-order planar Hall voltage $\Delta V_{\mathrm{PH}} = V_{\mathrm{PH}}(+I_{\mathrm{dc}}) + V_{\mathrm{PH}}(-I_{\mathrm{dc}})$ is measured while sweeping the external field H_{x} (Fig. 1(b)). The total current-induced in-plane transverse field H_{I} (which includes the Oersted field) pulls the magnetization away from the x-axis at an angle θ. When $|H_{\mathrm{x}}|$ is large enough ($\gtrsim$10 Oe) to magnetize the soft NiFe layer nearly uniformly, θ is small and ΔV_{PH} is proportional to $I_{\mathrm{dc}}^2 H_{\mathrm{x}}^{-1} dH_{\mathrm{I}}/dI_{\mathrm{dc}}$[10]. Following the procedure in Ref. 11 (with data at $|H_{\mathrm{x}}| < 10$ Oe discarded to eliminate spurious effects from nonuniform magnetization), we apply a constant transverse bias field $|H_{\mathrm{y}}| = 1$ Oe (Fig. 1(a),(b)) and extrapolate the critical H_{y} required to cancel H_{I}, i.e., to null the ΔV_{PH} spectrum. For the data in Fig. 1(b), H_{y} =-0.75 Oe would null ΔV_{PH}, so $H_{\mathrm{I}} = 0.75$ Oe at $I_{\mathrm{dc}} = 8$ mA.

As shown in Fig. 1(c), H_{I} scales linearly with I_{dc} with slope $\mathrm{d}H_{\mathrm{I}}/\mathrm{d}I_{\mathrm{dc}} = 0.095$ Oe per mA. To estimate the Oersted field contribution to H_{I}, the current is assumed to be uniform within each conductive layer, such that the Oersted field comes only from the current in the Ti layer, $H_{\mathrm{Oe,Ti}} = f_{\mathrm{Ti}} I_{\mathrm{dc}}/2w$, where f_{Ti} is the fraction of I_{dc} in Ti and w is the Hall bar width. The sheet resistances 2000 Ω/sq for Ti(1.2 nm) and 350 Ω/sq for NiFe(2.5 nm), found from four-point resistance measurements on a series of films (each with an insulating capping layer that prevents oxidation), yield $f_{\mathrm{Ti}} = 0.15$ and $|H_{\mathrm{Oe,Ti}}| = 0.009$ Oe per mA. The net H_{I} is therefore an order of magnitude larger than $H_{\mathrm{Oe,Ti}}$, and moreover, the direction of H_{I} opposes $H_{\mathrm{Oe,Ti}}$.

The actual Oersted field may deviate from $H_{\mathrm{Oe,Ti}}$ because of nonuniform current distribution within each conductive layer and interfacial scattering, both of which are difficult to quantify. However, we can place the upper bound on the Oersted field, $|H_{\mathrm{Oe,max}}| = |I_{\mathrm{dc}}|/2w$, by assuming that the *entire* I_{dc} flows above or below the magnetic layer. In Fig. 1(c), we shade the range bounded by $|H_{\mathrm{Oe,max}}|$. The magnitude of H_{I} still exceeds $H_{\mathrm{Oe,max}}$, confirming the presence of an additional current-induced field with a component collinear with the Oersted field.

We also measure H_{I} with a technique based on spin-torque ferromagnetic resonance (ST-FMR)[31,32]. As illustrated in Fig. 2(a), the rf excitation current is injected into a 5-μm wide, 25-μm long strip through a ground-signal-ground electrode. While the in-plane external field H is swept at an in-plane angle θ, the rectified mixing voltage V_{mix} across the strip is acquired with a lock-in amplifier[33]. The resulting spectrum (e.g., Fig. 2(b)) is well fit to a Lorentzian curve $V_{\mathrm{mix}} = V_{\mathrm{s}}F_{\mathrm{s}} + V_{\mathrm{a}}F_{\mathrm{a}}$ consisting of the symmetric component $F_{\mathrm{s}} = W^2/((H - H_{\mathrm{FMR}})^2 + W^2)$ and antisymmetric component $F_{\mathrm{a}} = W(H - H_{\mathrm{FMR}})/((H - H_{\mathrm{FMR}})^2 + W^2)$, where W is the resonance linewidth and H_{FMR} is the resonance field. We inject a small dc bias current $|I_{\mathrm{dc}}| \leq 2$ mA to measure the shift in H_{FMR} caused by the net I_{dc}-induced field H_{I}[33]. Although the scatter in the ST-FMR data is greater than the PHE data (Fig. 1(c)), Fig. 2(c) shows that the observed shift in H_{FMR} is significantly larger than (and opposes) the contribution from $H_{\mathrm{Oe,Ti}}$, and its magnitude exceeds the maximum possible shift from $H_{\mathrm{Oe,max}}$.

Fig. 2(d) shows the I_{dc}-induced shift ΔH_{FMR} as a function of in-plane magnetization angle, equal to the applied field angle θ for the soft NiFe layer. This angular dependence is well described by a $\sin\theta$ relation, which implies that H_{I} is transverse to the current axis. Fig. 2(e) shows that the constant $H_{\mathrm{I}} = -\Delta H_{\mathrm{FMR}}/\sin\theta$ indeed agrees well with the PHE data measured at $\theta \approx 0$. This finding confirms that H_{I}, including the non-Oersted contribution, is entirely transverse to the current and is independent of the magnetization orientation.

In Fig. 3(a), we plot the dependence of H_I (normalized by $H_{Oe,max}$ for clarity) on NiFe thickness t_{NiFe}. The two independent techniques, PHE at low applied fields and ST-FMR at high applied fields[34], confirm the presence of H_I that cannot be accounted for by the Oersted field alone for a wide range of t_{NiFe}. The observed H_{I} opposes $H_{\mathrm{Oe,Ti}}$ in all samples, and H_I is more than a factor of 2 larger than $H_{Oe,max}$ at $t_{NiFe} \approx 2$ nm. The drop in H_I for $t_{NiFe} \lesssim 2$ nm is caused by the increasing magnitude of $H_{Oe,Ti}$, as NiFe becomes more resistive and a larger fraction of current flows through Ti with decreasing t_{NiFe}.

The anomalous portion of H_I, which cannot be explained by the classical Oersted field, may be due to a spin-orbit torque that acts as a "spin-orbit field" H_{SO}. In Fig. 3(b), we plot the estimated $H_{SO} = H_I - H_{Oe,Ti}$ normalized by the current density in NiFe, J_{NiFe}. This normalized H_{SO} scales inversely with t_{NiFe}, implying that the source of H_{SO} is outside or at a surface of the NiFe layer. Therefore, H_{SO} does not arise from spin-orbit effects within the bulk of NiFe[35], i.e., the reciprocal of the recently reported inverse spin-Hall effect in FMs[36–39]. Moreover, any possible spin-orbit toques arising from the bulk of NiFe would depend on the magnetization orientation[35] and are thus incompatible with the observed symmetry of H_{SO} (Fig. 2(e)). It is unlikely that H_{SO} is generated by the spin-Hall effect in Ti, because its spin-Hall angle is small (<0.001)[40,41] and only a small fraction of I_{dc} is expected to be in the resistive ultrathin Ti layer. In Ti/NiFe/Al_2O_3, we also do not observe a damping-like torque that would be expected to arise from the spin-Hall effect[6,42]; the linewidth W is invariant with I_{dc} within our experimental resolution $\lesssim$0.2 Oe/mA[33].

With spin-orbit effects in the bulk of NiFe and Ti ruled out as mechanisms behind H_{SO}, the only known mechanism that agrees with the observed H_{SO} is the Rashba-Edelstein effect[1,4,5], with an interfacial spin accumulation (polarized transverse to the current) exchange coupling to the magnetization in NiFe. Indeed, tight-binding Rashba model calculations reveal a field-like torque, but no damping-like torque, in the first order of spin-orbit coupling due to transverse spin accumulation that is independent of the magnetization orientation[43].

We now gain further insight into the origin of H_{SO} by examining its dependence on the layer stack structure, as summarized in Fig. 4(a-f). In the symmetric Al_2O_3(1.5 nm)/NiFe(2.3 nm)/Al_2O_3(1.5 nm) trilayer (Fig. 4(a)), H_I vanishes, which is as expected because the Oersted field should be nearly zero and the two nominally identical interfaces sandwiching NiFe produces no net spin accumulation. Breaking structural inversion symmetry with the Ti(1.2 nm) seed layer results in an uncompensated interfacial spin accumulation that generates a finite $H_{SO} = H_I - H_{Oe,Ti}$ (Fig. 4(b)).

Inserting Pt(0.5 nm) between the NiFe and Al_2O_3 layers *suppresses* H_{SO}, such that the estimated Oersted field $H_{Oe,NM}$ from the nonmagnetic Ti and Pt layers entirely accounts for H_I (Fig. 4(c)). This may seem counterintuitive since Pt exhibits strong spin-orbit coupling and a large Rashba-Edelstein effect may be expected[44]. However, Pt is also a strong spin scatterer, as evidenced by an increase in the Gilbert damping parameter from ≈0.013 for Ti/NiFe/Al_2O_3 to ≈0.03 for Ti/NiFe/Pt/Al_2O_3. Any accumulated spins may quickly become scattered by Pt, such that there is no net field-like torque mediated by exchange coupling[4,5] between these spins and the magnetization in NiFe[45]. Based on the suppression of H_{SO} by Pt insertion, we infer that the Rashba-Edelstein effect at the NiFe/Al_2O_3 interface is the source of H_{SO}.

We observe another unexpected result upon inserting a layer of Cu, a metal with nearly zero bulk spin-orbit coupling, at the NiFe/Al_2O_3 interface: The direction of $H_{SO} = H_I - H_{Oe,NM}$ is *reversed* (Fig. 4(d)). Just as in Ti/NiFe/Al_2O_3, this observed H_{SO} in Ti/NiFe/Cu/Al_2O_3 is independent of magnetization orientation, and no damping-like torque is detected within our experimental resolution. We deduce a Rashba-Edelstein effect (opposite in sign to that of NiFe/Al_2O_3) at the Cu/Al_2O_3 interface, rather than the NiFe/Cu interface, because (1) if NiFe/Cu generates the reversed H_{SO}, we should see an enhanced H_{SO} for NiFe sandwiched between Cu (bottom) and Al_2O_3 (top), but this is not the case (Fig. 4(e)); and (2) inserting a spin-scattering layer of Pt(0.5 nm) between Cu and Al_2O_3 suppresses H_{SO} (Fig. 4(f)). Fig. 4(g) plots the dependence of H_I on Cu thickness t_{Cu}. In the limit of large t_{Cu} (≈10 nm), H_I approaches $H_{Oe,NM}$ that is predominantly due to the current in the highly conductive Cu layer. From the estimated current distribution, we obtain $H_{SO} = H_I - H_{Oe,NM}$ normalized by the current density in the Cu layer, J_{Cu}. As shown in Fig. 4(h), $H_{SO}/J_{Cu} \approx$ 1-2 Oe/10^{11} A/m^2 exhibits little dependence on t_{Cu}. This is consistent with the Rashba-Edelstein effect at the Cu/Al_2O_3 interface that is present irrespective of t_{Cu}.

Persistence of H_{SO} even at large t_{Cu} indicates a nonlocal Rashba-Edelstein field, whereas the absence of a damping-like torque implies negligible diffusive (dissipative) spin transport from the Cu/Al_2O_3 interface to the NiFe layer. Evidently, the spin accumulation at the Cu/Al_2O_3 interface exchange couples to the magnetization in NiFe across the Cu layer. However, further studies are required to elucidate the mechanism involving Cu, since we do not observe any apparent oscillation in H_{SO} with t_{Cu} that would be expected for exchange coupling across Cu[46]. Theoretical studies may also clarify why the directions of H_{SO} arising from NiFe/Al_2O_3 and Cu/Al_2O_3 are opposite. Another outstanding question that can be addressed by further experimental work is how the level of oxidation or disorder at the metal/insulator interface influences H_{SO}.

At $t_{Cu} \approx 2$ nm, H_I vanishes because H_{SO} and $H_{Oe,NM}$ compensate each other (Fig. 4(g)). Fan *et al.* also show near vanishing of H_I in NiFe(2 nm)/Cu(t_{Cu})/SOi_2(3.5 nm) at $t_{Cu} \approx 3$ nm[10], and Avci *et al.* report a current-induced field in Co(2.5 nm)/Cu(6 nm)/AlO_x(1 nm) that is well below the estimated Oersted field[20]. In each of these studies[10,20], a spin-orbit field due to the Rashba-Edelstein effect at the Cu/oxide interface may have counteracted the Oersted field. More generally, various metal/insulator interfaces, where the metal is ferromagnetic or nonmagnetic, may exhibit Rashba-Edelstein effects. In some HM/FM/oxide heterostructures, the Rashba-Edelstein torque from the FM/oxide interface may even dominate over torques from the HM bulk or HM/FM interface, e.g., when the HM is thin and hence resistive, which possibly explains the reported sign reversal in the field-like torque with decreasing HM thickness[13,19].

In summary, we have shown a current-induced spin-orbit torque due to Rashba-Edelstein effects at NiFe/Al_2O_3 and Cu/Al_2O_3 interfaces. This torque is distinct from previously reported spin-orbit torques in that it arises even without spin-orbit coupling in the bulk of the constituent materials. The origin of this torque is purely interfacial spin-orbit coupling, which likely emerges from the electric dipoles that develop at the metal/insulator interfaces[29,30]. This mechanism is supported by recent theoretical predictions of current-induced spin polarization at metal/insulator interfaces in the absence of bulk spin-orbit coupling[47–49]. Rashba-Edelstein effects at metal/insulator interfaces may be universal and should motivate the use of various previously neglected materials as components for enhancing spin-orbit torques and as model systems for interfacial spin-dependent physics, perhaps combined with gate-voltage tuning[21,22,50]. One possibility is to apply interfacial band alignment techniques, similar to those for semiconductor heterostructures[51], to control dipole-induced Rashba-Edelstein effects.

This work was supported by the AFRL through contract FA8650-14-C-5706, the W.M. Keck Foundation, and the NSF TANMS ERC Award 1160504. X-ray reflectivity was performed in CMSE at MIT, and lithography was performed in the George J. Kostas Nanoscale Technology and Manufacturing Research Center. We thank Geoffrey Beach, Carl Boone, Xin Fan, Adrian Feiguin, Chi-Feng Pai, and Kohei Ueda for helpful discussions. We give special thanks to Mairbek Chshiev, Sergey Nikolaev, and Noriyuki Sato for their comments

and sharing of unpublished results.

---

* Current Address: Geballe Laboratory for Advanced Materials, Stanford University, Stanford, CA 94305 USA ; satorue@stanford.edu

† Current Address: Department of Materials Science and Engineering, University of Wisconsin Madison, Madison, WI 53706 USA

[1] V. Edelstein, Solid State Commun. **73**, 233 (1990).

[2] A. Hoffmann, IEEE Trans. Magn. **49**, 5172 (2013).

[3] J. Sinova, S. O. Valenzuela, J. Wunderlich, C. H. Back, and T. Jungwirth, Rev. Mod. Phys. **87**, 1213 (2015).

[4] A. Manchon and S. Zhang, Phys. Rev. B **78**, 212405 (2008).

[5] P. Gambardella and I. M. Miron, Philos. Trans. A. Math. Phys. Eng. Sci. **369**, 3175 (2011).

[6] P. M. Haney, H.-W. Lee, K.-J. Lee, A. Manchon, and M. D. Stiles, Phys. Rev. B **87**, 174411 (2013).

[7] A. Brataas and K. M. D. Hals, Nat. Nanotechnol. **9**, 86 (2014).

[8] A. Chernyshov, M. Overby, X. Liu, J. K. Furdyna, Y. Lyanda-Geller, and L. P. Rokhinson, Nat. Phys. **5**, 656 (2009).

[9] L. Liu, O. J. Lee, T. J. Gudmundsen, D. C. Ralph, and R. A. Buhrman, Phys. Rev. Lett. **109**, 096602 (2012).

[10] X. Fan, J. Wu, Y. Chen, M. J. Jerry, H. Zhang, and J. Q. Xiao, Nat. Commun. **4**, 1799 (2013).

[11] X. Fan, H. Celik, J. Wu, C. Ni, K.-J. Lee, V. O. Lorenz, and J. Q. Xiao, Nat. Commun. **5**, 3042 (2014).

[12] C.-F. Pai, M.-H. Nguyen, C. Belvin, L. H. Vilela-Leão, D. C. Ralph, and R. A. Buhrman, Appl. Phys. Lett. **104**, 082407 (2014).

[13] M.-H. Nguyen, D. C. Ralph, and R. A. Buhrman, Phys. Rev. Lett. **116**, 126601 (2016).

[14] I. M. Miron, K. Garello, G. Gaudin, P.-J. Zermatten, M. V. Costache, S. Auffret, S. Bandiera, B. Rodmacq, A. Schuhl, and P. Gambardella, Nature **476**, 189 (2011).

[15] T. D. Skinner, M. Wang, A. T. Hindmarch, A. W. Rushforth, A. C. Irvine, D. Heiss, H. Kurebayashi, and A. J. Ferguson, Appl. Phys. Lett. **104**, 062401 (2014).

[16] M. Kawaguchi, T. Moriyama, T. Koyama, D. Chiba, and T. Ono, J. Appl. Phys. **117**, 17C730

(2015).

[17] G. Allen, S. Manipatruni, D. E. Nikonov, M. Doczy, and I. A. Young, Phys. Rev. B **91**, 144412 (2015).

[18] K. Garello, I. M. Miron, C. O. Avci, F. Freimuth, Y. Mokrousov, S. Blügel, S. Auffret, O. Boulle, G. Gaudin, and P. Gambardella, Nat. Nanotechnol. **8**, 587 (2013).

[19] J. Kim, J. Sinha, M. Hayashi, M. Yamanouchi, S. Fukami, T. Suzuki, S. Mitani, and H. Ohno, Nat. Mater. **12**, 240 (2013).

[20] C. O. Avci, K. Garello, M. Gabureac, A. Ghosh, A. Fuhrer, S. F. Alvarado, and P. Gambardella, Phys. Rev. B **90**, 224427 (2014).

[21] R. H. Liu, W. L. Lim, and S. Urazhdin, Phys. Rev. B **89**, 220409 (2014).

[22] S. Emori, U. Bauer, S. Woo, and G. S. D. Beach, Appl. Phys. Lett. **105**, 222401 (2014).

[23] X. Qiu, K. Narayanapillai, Y. Wu, P. Deorani, D.-H. Yang, W.-S. Noh, J.-H. Park, K.-J. Lee, H.-W. Lee, and H. Yang, Nat. Nanotechnol. **10**, 333 (2015).

[24] M. Akyol, G. Yu, J. G. Alzate, P. Upadhyaya, X. Li, K. L. Wong, A. Ekicibil, P. Khalili Amiri, and K. L. Wang, Appl. Phys. Lett. **106**, 162409 (2015).

[25] N. Sato, A. El-Ghazaly, R. M. White, and S. X. Wang, to be published in IEEE. Trans. Magn. (2016).

[26] J. C. Rojas Sánchez, L. Vila, G. Desfonds, S. Gambarelli, J. P. Attané, J. M. De Teresa, C. Magén, and A. Fert, Nat. Commun. **4** (2013).

[27] K. Chen and S. Zhang, Phys. Rev. Lett. **114**, 126602 (2015).

[28] W. Zhang, M. B. Jungfleisch, W. Jiang, Y. Liu, J. E. Pearson, S. G. E. te Velthuis, A. Hoffmann, F. Freimuth, and Y. Mokrousov, Phys. Rev. B **91**, 115316 (2015).

[29] L. Xu and S. Zhang, J. Appl. Phys. **111**, 07C501 (2012).

[30] F. Ibrahim, H. X. Yang, A. Hallal, B. Dieny, and M. Chshiev, Phys. Rev. B **93**, 014429 (2016).

[31] L. Liu, T. Moriyama, D. C. Ralph, and R. A. Buhrman, Phys. Rev. Lett. **106**, 036601 (2011).

[32] D. Fang, H. Kurebayashi, J. Wunderlich, K. Výborný, L. P. Zârbo, R. P. Campion, A. Casiraghi, B. L. Gallagher, T. Jungwirth, and A. J. Ferguson, Nat. Nanotechnol. **6**, 413 (2011).

[33] T. Nan, S. Emori, C. T. Boone, X. Wang, T. M. Oxholm, J. G. Jones, B. M. Howe, G. J. Brown, and N. X. Sun, Phys. Rev. B **91**, 214416 (2015).

[34] ST-FMR is conducted with maximum $H = 800$ Oe. No dependence of H_I on H (or excitation frequency) was observed.

[35] T. Taniguchi, J. Grollier, and M. D. Stiles, Phys. Rev. Appl. **3**, 044001 (2015).

[36] B. F. Miao, S. Y. Huang, D. Qu, and C. L. Chien, Phys. Rev. Lett. **111**, 066602 (2013).

[37] A. Tsukahara, Y. Ando, Y. Kitamura, H. Emoto, E. Shikoh, M. P. Delmo, T. Shinjo, and M. Shiraishi, Phys. Rev. B **89**, 235317 (2014).

[38] A. Azevedo, O. Alves Santos, R. O. Cunha, R. Rodríguez-Suárez, and S. M. Rezende, Appl. Phys. Lett. **104**, 152408 (2014).

[39] H. Wang, C. Du, P. Chris Hammel, and F. Yang, Appl. Phys. Lett. **104**, 202405 (2014).

[40] C. Du, H. Wang, F. Yang, and P. C. Hammel, Phys. Rev. B **90**, 140407 (2014).

[41] K. Uchida, M. Ishida, T. Kikkawa, A. Kirihara, T. Murakami, and E. Saitoh, J. Phys. Condens. Matter **26**, 343202 (2014).

[42] F. Freimuth, S. Blügel, and Y. Mokrousov, Phys. Rev. B **90**, 174423 (2014).

[43] A. Kalitsov, S. A. Nikolaev, J. Velev, W. H. Butler, M. Chshiev, and O. Mryasov, unpublished (2016).

[44] H. J. Zhang, S. Yamamoto, Y. Fukaya, M. Maekawa, H. Li, A. Kawasuso, T. Seki, E. Saitoh, and K. Takanashi, Sci. Rep. **4** (2014).

[45] With the insertion of Pt(0.5 nm), while the field-like torque is suppressed, a small damping-like torque emerges with an estimated effective spin-Hall angle θ_{DL} (defined in [33]) of ≈0.01.

[46] S. S. P. Parkin, Phys. Rev. Lett. **67**, 3598 (1991).

[47] X. Wang, J. Xiao, A. Manchon, and S. Maekawa, Phys. Rev. B **87**, 081407 (2013).

[48] J. Borge, C. Gorini, G. Vignale, and R. Raimondi, Phys. Rev. B **89**, 245443 (2014).

[49] S. S.-L. Zhang, G. Vignale, and S. Zhang, Phys. Rev. B **92**, 024412 (2015).

[50] U. Bauer, L. Yao, A. J. Tan, P. Agrawal, S. Emori, H. L. Tuller, S. van Dijken, and G. S. D. Beach, Nat. Mater. **14**, 174 (2015).

[51] H. Kroemer, Rev. Mod. Phys. **73**, 783 (2001).

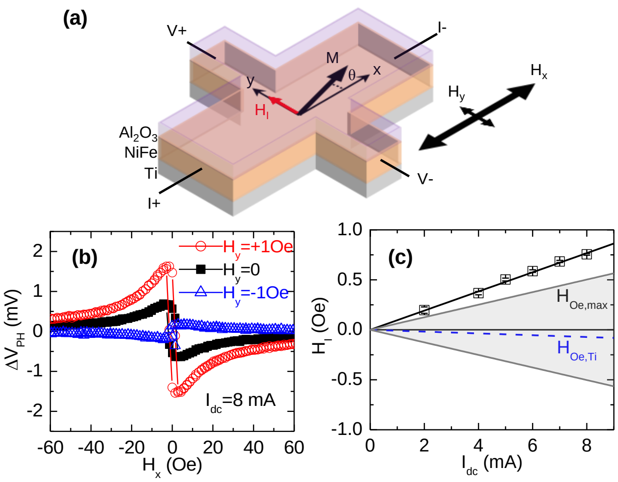

Figure 1. (a) Schematic of the second-order PHE measurement. (b) Second-order planar Hall voltage ΔV_{PH} curves at different transverse bias fields H_{y}. (c) Current-induced field H_{I} versus I_{dc}. The dotted line shows $H_{\mathrm{Oe,Ti}}$ based on the estimated fraction of I_{dc} in Ti. The shaded area is bounded by the maximum possible Oersted field $H_{\mathrm{Oe,max}}$.

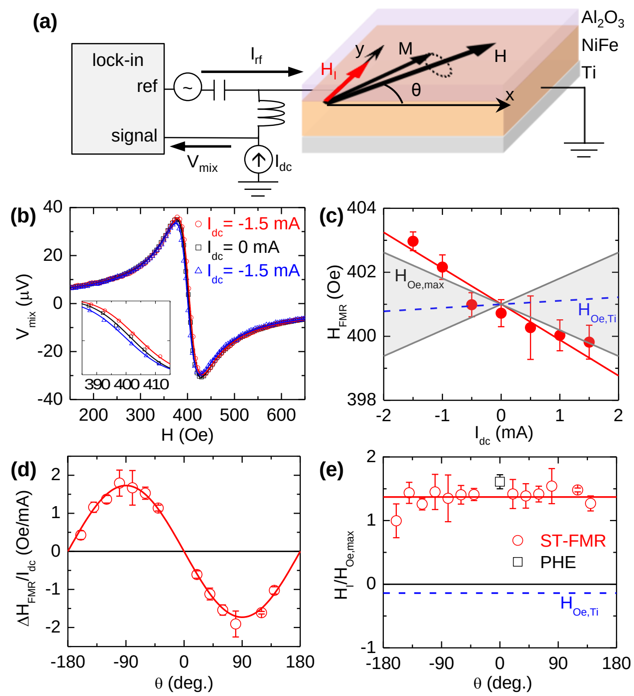

Figure 2. (a) Schematic of the ST-FMR setup. (b) ST-FMR spectra at different dc bias currents $I_{\rm dc}$, with rf current excitation at 5 GHz and +8 dBm and external field H at $\theta = 40°$. Inset: $I_{\rm dc}$-induced shift of ST-FMR spectra. (c) Shift of resonance field $H_{\rm FMR}$ due to $I_{\rm dc}$ at $\theta = 40°$. The error bar is the standard deviation of 5 measurements. The dotted line shows the estimated Oersted field from Ti, $H_{\rm Oe,Ti}$. The shaded area is bounded by the maximum possible Oersted field, $H_{\rm Oe,max}$. (d) Angular dependence of $I_{\rm dc}$-induced $H_{\rm FMR}$ shift. The solid curve indicates the fit to $\sin\theta$. (e) Transverse current-induced field $H_{\rm I} = -\Delta H_{\rm FMR}/\sin\theta$ normalized by $H_{\rm Oe,max}$ at various θ. The error bar is the error in linear fit of $H_{\rm FMR}$ versus $I_{\rm dc}$. The solid line indicates the average of the ST-FMR data points. The dotted line indicates estimated $H_{\rm Oe,Ti}$. The PHE data point at $\theta = 0$ is the average of three devices.

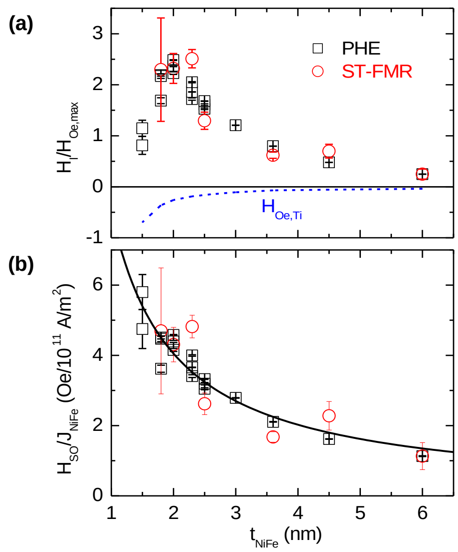

Figure 3. (a) NiFe-thickness t_{NiFe} dependence of H_{I} normalized by $H_{\mathrm{Oe,max}}$. The dotted curve indicates the estimated Oersted field from Ti, $H_{\mathrm{Oe,Ti}}$. Each ST-FMR data point is the mean of results at several frequencies 3.5-7.0 GHz at $\theta = 45^\circ$ and -135°. $H_{\mathrm{I}}/H_{\mathrm{Oe,max}} > 0$ is defined as $H_{\mathrm{I}} /\!/ +y$ when $I_{\mathrm{dc}} /\!/ +x$ (illustrated in Figs. 1(a) and 2(a)). (b) Estimated spin-orbit field H_{SO} per unit current density in NiFe, J_{NiFe}. The solid curve indicates the fit to $t_{\mathrm{NiFe}}{}^{-1}$.

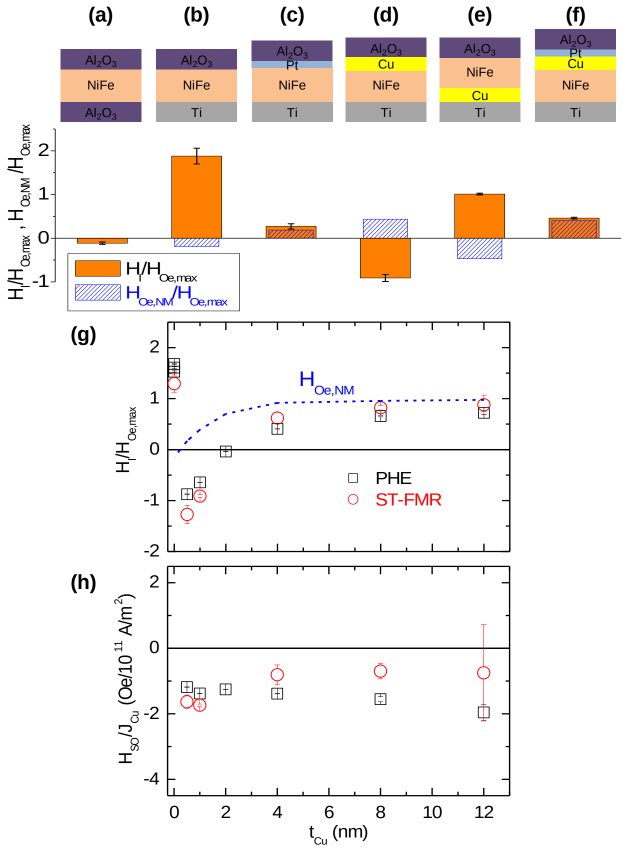

Figure 4. (a-f) Structural dependence of H_I (mean of measurements on three PHE devices) normalized by $H_\mathrm{Oe,max}$. $H_\mathrm{Oe,NM}$ is the Oersted field from current in the nonmagnetic metal layers (Ti, Cu, Pt). The nominal layer thicknesses are NiFe: 2.3 nm, Al_2O_3: 1.5 nm, Ti: 1.2 nm, Cu: 1.0 nm, and Pt: 0.5 nm. (g) Cu-thickness t_Cu dependence of H_I normalized by $H_\mathrm{Oe,max}$ at NiFe thickness 2.5 nm. The blue dotted curve indicates $H_\mathrm{Oe,NM}$. (h) Estimated spin-orbit field H_SO per unit current density in Cu, J_Cu.